

UCSF

UC San Francisco Previously Published Works

Title

Hydrogel Magnetomechanical Actuator Nanoparticles for Wireless Remote Control of Mechanosignaling In Vivo

Permalink

<https://escholarship.org/uc/item/9324c07j>

Journal

Nano Letters, 23(11)

ISSN

1530-6984

Authors

Jeong, Sumin
Shin, Wookjin
Park, Mansoo
[et al.](#)

Publication Date

2023-06-14

DOI

10.1021/acs.nanolett.3c01207

Copyright Information

This work is made available under the terms of a Creative Commons Attribution License, available at <https://creativecommons.org/licenses/by/4.0/>

Peer reviewed

Hydrogel magnetomechanical actuator (h-MMA) nanoparticles for wireless remote control of mechanosignaling *in vivo*

Sumin Jeong^{1,2,‡}, Wookjin Shin^{1,‡}, Mansoo Park^{1,3}, Jung-uk Lee¹, Yongjun Lim^{1,2}, Kunwoo Noh^{1,3}, Jae-Hyun Lee^{1,3}, Young-wook Jun^{1,3,4,5,6,*}, Minsuk Kwak^{1,3,*} & Jinwoo Cheon^{1,2,3,*}

¹ Center for Nanomedicine, Institute for Basic Science (IBS), Seoul 03722, Republic of Korea

² Department of Chemistry, Yonsei University, Seoul 03722, Republic of Korea

³ Department of Nano Biomedical Engineering (NanoBME), Advanced Science Institute, Yonsei University, Seoul 03722, Republic of Korea

⁴ Department of Otolaryngology, University of California, San Francisco, CA, USA

⁵ Department of Pharmaceutical Chemistry, University of California, San Francisco, CA, USA

⁶ Helen Diller Family Cancer Comprehensive Center (HDFCCC), University of California, San Francisco, CA, USA

‡ These authors contributed equally to this work.

*e-mail: young-wook.jun@ucsf.edu, minsuk.kwak@yonsei.ac.kr, or jcheon@yonsei.ac.kr

Keywords: magnetic nanoparticle cluster, magnetic hyperthermia effect, thermoresponsive hydrogel, mechanosensitive receptor, perturbation biology

1 **Abstract**

2 As a new enabling nanotechnology tool for wireless, target-specific, and long-distance stimulation of
3 mechanoreceptors *in vivo*, here we present a hydrogel magnetomechanical actuator (h-MMA) nanoparticle. To
4 allow both deep-tissue penetration of input signals and efficient force-generation, h-MMA integrates a two-
5 step transduction mechanism that converts magnetic anisotropic energy to thermal energy within its magnetic
6 core (*i.e.*, $\text{Zn}_{0.4}\text{Fe}_{2.6}\text{O}_4$ nanoparticle cluster) and then mechanical energy to induce the surrounding polymer
7 (*i.e.*, pNiPMAM) shell contraction, finally delivering forces to activate targeted mechanoreceptors. We show
8 that h-MMAs enable on-demand modulation of Notch signaling in both fluorescence reporter cell lines and a
9 xenograft mouse model, demonstrating the utility as a powerful *in vivo* perturbation approach for
10 mechanobiology interrogation in a minimally invasive and untethered manner.

11

1 Tools for manipulating signaling, activity, and function of specific cells in living organisms have enormous
2 potential to promote novel perturbation biology approaches and unprecedented therapeutic strategies^{1,4}. The
3 past decades have witnessed a drastic expansion in physical perturbation methods including nano/micro-
4 electrode arrays^{5,6}, microfluidics^{7,8}, optogenetics⁹⁻¹¹, upconversion nanoparticles¹²⁻¹⁵, thermogenetic¹⁶⁻²⁰,
5 sonogenetics^{21,22}, and mechanogenetics^{23,24}, enabling neuromodulation, stem cell differentiation, immune cell
6 activation, and cell migration and adhesion with high spatiotemporal precision. However, despite the potential,
7 broad *in vivo* applications of these tools have been lagged by technical limitations. Electrode- or light-based
8 techniques require device implementation into target tissues due to the low tissue penetration depth of input
9 signals^{25,26}. Mechanogenetic tools based on force exerted by single magnetic particles under magnetic field
10 gradient only allow short-distance operation, incompatible with animal studies^{27,28}. On the other hand, the use
11 of alternating or rotational magnetic field with uniform strength offers long-range stimulation of targeted
12 receptors by converting magnetic anisotropy energy to thermal energy or torque, as demonstrated in magneto-
13 thermogenetic and m-Torquer regulation of specific channel proteins including TRPV and Piezo1,
14 respectively²⁹⁻³². The development of a new tool, that exploits the long-distance operation of the uniform
15 magnetic field while converting the magnetic energy to a different form of physical cue beyond heat or torque,
16 will greatly enhance its useability and applicability to diverse cell signaling processes.

17 We particularly sought to develop a hydrogel magnetomechanical actuator (h-MMA) nanoparticle
18 that eventually exerts mechanical tensile stress to target proteins in response to oscillatory magnetic field
19 stimulation, as many mechanosensitive proteins relay the signal by unfolding the force-sensing domain upon
20 the application of mechanical pulling³³⁻³⁸. Since the direct conversion of magnetic anisotropy energy to
21 mechanical pulling is difficult, we employed a two-step mechanism – magnetic-to-thermal and thermal-to-
22 mechanical transductions, wherein each transduction could be more straightforward by using magnetic
23 nanoparticles and thermosensitive hydrogel polymers, respectively (**Fig. 1a**)³⁹⁻⁶¹. Specifically, we designed an
24 h-MMA comprised of a magnetic nanoparticle cluster (MNC) core surrounded by a poly N-
25 isopropylmethylacrylamide (pNiPMAM) shell layer. We chose the MNC core to maximize heat generation per
26 particle, while effectively localizing the energy to its surrounding shell layer (detailed discussion in Fig. 2).
27 We also chose pNiPMAM as the shell layer of h-MMA, because of its volume-phase-transition (VPT)
28 behaviors ideally suited for the envisioned application, which include 1) drastic size reduction (up to 75 %)
29 upon VPT, 2) tunable critical transition temperature (T_c) near the body temperature, and 3) facile bio-
30 functionalization. To fabricate h-MMA, we first assembled 13 nm Zn-doped iron oxide ($Zn_{0.4}Fe_{2.6}O_4$)
31 nanoparticles into a superlattice via oil-in-water microemulsion entrapping followed by evaporating the low-
32 boiling point solvent in the oil phase⁶²⁻⁶⁶. MNCs were coated with a thin SiO_2 (~10 nm) layer and then
33 pNiPMAM via the Stöber method and radical polymerization, respectively (**Fig. 1b**, See methods for details)⁶⁷.

1 **Figure 1c** shows representative transmission electron microscope (TEM) images and dynamic light scattering
2 analysis (inset) of MNCs (TEM: 238 ± 28.2 nm, hydrodynamic size: 284 ± 45.1 nm), MNC@SiO₂ (TEM: 260
3 ± 37.8 nm, hydrodynamic size: 302 ± 83.1 nm), and MNC@SiO₂@pNiPMAM (TEM: 700 ± 50.2 nm,
4 hydrodynamic size: 817 ± 198 nm), confirming the high quality of particles with respect to cluster, size and
5 shape uniformity, and colloidal stability, where these parameters were important for the desired downstream
6 application. To estimate the number density of Zn_{0.4}Fe_{2.6}O₄ nanoparticles per MNC, we performed tilted-angle
7 TEM analyses of MNCs along different superlattice crystallographic directions. MNCs have a face-centered-
8 cubic (FCC) cluster with a lattice constant of 20.8 nm suggesting approximately 3,136 particles per MNC (**Fig.**
9 **1d**). The FCC-structured MNCs exhibit maximized nanoparticle packing density (4.44×10^5 particles per μm^3)
10 and therefore higher magnetization (1.249 pemu per MNC @500 Oe), compared to random aggregate
11 counterparts (3.60×10^5 particles per μm^3 , 0.982 pemu per random aggregate @500 Oe) (**Fig. S1**).
12 Accordingly, when assessed magnetic-to-thermal energy conversion capacity via calorimetric bulk solution
13 heating measurement under the application of alternating magnetic fields (AMF at 500 kHz, 500 Oe), a single
14 MNC particle generated approximately 6.83 pW of individual particle power loss (IPLP), 2800 and 1.34 times
15 stronger than a single Zn_{0.4}Fe_{2.6}O₄ nanoparticle (2.44 fW) and a random aggregate (5.08 pW), respectively
16 (**Fig. 1e, Fig. S2, Supplementary Note 1**).

17 We next tested the capacity of h-MMA (*i.e.*, MNC@SiO₂@pNiPMAM) to transduce heat to
18 mechanical motion by measuring its hydrodynamic size via dynamic light scattering (DLS) while gradually
19 increasing the bulk solution temperature. h-MMA exhibited a clear VPT near 43 °C (*i.e.*, T_c), where the
20 hydrodynamic size gradually decreases from approximately 858 nm to 556 nm with increasing temperature
21 from 30 to 60 °C, respectively, suggesting the collapse of the pNiPMAM layer to 64.8 % of the original size
22 (**Fig. 1f**)^{9,58,60,68}. h-MMA showed stable (variance of the size < 30 nm @ 30 °C with no aggregation), reversible,
23 and sustained VPT behaviors during repeated temperature cycles between 30 °C to 60 °C, confirming the high
24 performance of h-MMAs as thermal-to-mechanical transduction (**Fig. 1g, Fig. S3**). Previous studies have
25 reported that nanoscale heating of the particle core leads to volume-phase transition of pNiPMAM and the
26 collapse of hydrogel particles on the time scale of ~100 nanoseconds, which allows for h-MMA applications
27 of pN force^{58,60}.

28 Together, these two transduction experiments (*i.e.*, AMF-to-bulk heating and bulk heating-to-h-MMA
29 contraction) indicate that h-MMAs are capable of converting an AMF input to the mechanical output signal
30 *via* bulk solution heating using high particle concentration. However, prolonged bulk heating can cause many
31 undesired consequences including cell/tissue damage, nonspecific activation of thermosensitive receptors, and
32 perturbation of extracellular environments. We previously showed that, at a low particle concentration (0.1
33 mg/ml), magnetic nanoparticle (*i.e.*, 15 nm CoFe₂O₄@MnFe₂O₄) produced local and transient heating to its

1 vicinity (< 10 nm) (**Fig. S4**), finally facilitating radical polymerization of vinyl monomers⁶⁹. We hypothesized
2 that the MNC core could induce local heating with more extended ranges, while minimally influencing bulk
3 solution temperature. To test this hypothesis, we synthesized a set of MNC@SiO₂ particles with varied SiO₂
4 layer thickness (d) of approximately 10 (9.7 ± 2.5), 21 (21.4 ± 3.2), 38 (38.3 ± 3.8), and 65 (64.8 ± 5.5) nm,
5 and induced radical polymerization of N-(2-aminoethyl)methacrylate (AEM) under AMF application (500
6 kHz at 500 Oe, 30 min ON / 30 min OFF cycle for 4 times; **Fig. 2a, Fig. S6**). We employed a series of
7 thermo-labile azo-molecule radical initiators (initiators A-C) with varied degradation temperatures of 66, 78,
8 and 102 °C at a given experimental condition, respectively (**Fig. 2a**)^{70,71}. We then assessed poly-AEM (p AEM)
9 formation on MNC@SiO₂ particles by TEM (**Fig. 2b**). When d equals or below 38 nm and initiators A or B
10 were used, we observed the formation of an additional contrasted layer on MNC@SiO₂, presumably
11 corresponding to p AEM. With the initiator C, however, we observed no changes compared with original
12 MNC@SiO₂ particles, suggesting that temperature reached 78 °C but was below 102 °C at $d \leq 38$ nm. When
13 $d = 65$ nm, we detected the contrasted layer for initiators A but not for B or C, indicating that the temperature
14 at this distance range is approximately 66-78 °C. To test whether the contrasted layer in TEM corresponds to
15 p AEM or not, we further reacted as-synthesized particles with amine-reactive fluorescence dyes (Alexa 488-
16 NHS) and counted fluorescence-positive fractions for respective MNC@SiO₂ and initiator combinations under
17 fluorescence microscopy (**Fig. 2c, d, Fig. S7**). Since the original MNC@SiO₂ particle has no amine functional
18 group but p AEM does, positive fluorescence signals after Alexa 488-NHS treatment indicate the p AEM layer
19 formation. We observed fluorescence-positive particles only from the samples with the silica thickness and
20 initiator combinations that show additional contrasted layers under TEM, confirming the formation of p AEM
21 shells (**Fig. 2d, Fig. S7**). During AMF stimulation, changes in bulk solution temperature was minimal (**Fig.**
22 **S5**). While exact distance-dependent temperature decay profiles from the MNC core remained to be
23 determined, these results confirm that AMF stimulation of MNC can induce significant local heating (> 60 °C)
24 over 60 nm distance ranges from the MNC surface. These results also suggest that AMF stimulation of h-
25 MMA (*i.e.*, MNC@SiO₂@pNiPMAM) can induce VPT ($T_c = 43$ °C) of a substantial portion of the
26 thermoresponsive layer (*i.e.*, pNiPMAM).

27 We next examined whether h-MMAs can be used for the envisioned application: target-specific and
28 long-range stimulation of mechanosensitive receptors in cells. As an initial study, we applied h-MMAs to
29 control Notch1 signaling in a cell culture model. We previously showed that Notch1 is a true mechanoreceptor,
30 where mechanogenetic stimulation of Notch1 resulted in its cell surface activation and downstream
31 signaling^{24,72,73}. We hypothesized that, when targeted to Notch1, h-MMAs can provide the same function while
32 allowing long-range stimulation. To allow bio-targeting, fluorescence imaging, and minimal nonspecific
33 binding, we conjugated h-MMAs with single-stranded oligonucleotides, fluorescence dyes (Alexa 488), and

1 polyethylene glycol (PEG), respectively, via click chemistry (see Method sections for details). We then treated
2 a fluorescence reporter U2OS cell line expressing SNAP-Notch1-Gal4 and UAS-H2B-mCherry with
3 benzylguanine-functionalized oligonucleotides bearing complementary sequences (BG-DNA) and oligo-
4 conjugated h-MMAs, sequentially (**Fig. 3a**). Robust green fluorescence signals were seen at the cell
5 membrane under confocal fluorescence microscopy, suggesting the surface labeling of cells with h-MMA (**Fig.**
6 **S6**). Control groups without BG-DNA, using h-MMAs without azide oligonucleotides, or using U2OS cells
7 not expressing SNAP-Notch1 showed negligible fluorescence, confirming target-specific h-MMA labeling
8 (**Fig. S8**). We then applied AMF (500 kHz at 500 Oe, 30 s ON / 2 min OFF cycle for 15 times, **Fig. S9-11, S15**)
9 and measured reporter mCherry signals of the cells 24 hr post-stimulation (**Fig. 3a**). Cells treated with h-
10 MMA and AMF stimulation showed robust nuclear mCherry signals (56.8% mCherry-positive cell fraction;
11 13.9-fold mean fluorescence intensity) comparable to the cells with Notch receptor-ligand engagement, while
12 those treated with h-MMA (1.38 %; 0.63-fold) or AMF (1.29 %; 0.80-fold) alone showed negligible nuclear
13 fluorescence (**Fig. 3b-d, Fig. S12-15**)^{72,74}. The pNiPMAM particle collapse in response to alternating
14 magnetic field stimulation exerts > 13 pN force per receptor, which is adequate to mechanically activate
15 Notch1^{9,24,73}. To directly assess surface activation of Notch, we performed a Western immunoblotting assay
16 that detects cleaved Notch intracellular domain (NICD). Cells treated with both h-MMA and AMF stimulation
17 produced a significantly increased amount of NICD (6.60-fold) compared to the control groups (**Fig. 3e**). *In*
18 *vitro* AMF stimulation resulted in minimal bulk solution heating (< 1°C), which has no effect on cell signaling
19 or on cell viability (**Fig. S16, 17**). These results demonstrate the capacity of h-MMA for specific and targeted
20 stimulation of cells expressing mechanoreceptors.

21 To demonstrate *in vivo* translation of these successful *in vitro* experiments, we next generated a
22 xenograft mouse model implanted with fluorescence reporter Notch1-U2OS cells described above (**Fig. 4a**).
23 To establish a bilateral tumor model, 4×10^6 SNAP-Notch1-Gal4 and UAS-H2B-mCherry expressing U2OS
24 cells were subcutaneously implanted into both sides. Mice were provided with the doxycycline (Dox) diet (2
25 mg/mL) for 8 days to induce robust Notch1 expression in the xenografts (**Fig. S18**). We injected BG-
26 conjugated h-MMAs intratumorally to the left xenograft site locally, while 30 cycles of AMF stimulation (30 s
27 ON / 2 min OFF for total 75 min) were applied to both sites (**Fig. 4a, Fig. S19**). After 24 hrs, we sacrificed
28 mice and extracted both tumor masses for immunofluorescence analysis. To detect nuclear mCherry
29 expression, tumors were cryosectioned, immunostained with anti-mCherry antibodies, and imaged under
30 confocal fluorescence microscopy. Consistent with the *in vitro* results, we observed robust mCherry
31 fluorescence signals from the tumor treated with h-MMA and AMF but negligible signals from control groups
32 without Dox, BG-h-MMAs, or applied AMF (**Fig. 4b-d**), supporting the capacity of h-MMAs for target- and
33 AMF-specific modulation of mechanoreceptors *in vivo*. To test whether h-MMA causes side effects, we

1 evaluated tissue inflammation and toxicity by immunohistochemical analyses against Iba1. No cytotoxicity or
2 tissue inflammation was seen due to h-MMAs and/or AMF stimulation *in vivo* (**Fig. S20, 21**). While
3 promising, biodistribution and systematic clearance of h-MMA have remained to be investigated for its
4 potential clinical uses.

5 In summary, we developed a novel *in vivo* perturbation platform based on h-MMA nanoparticles. We
6 demonstrated that h-MMA nanoparticles effectively convert magnetic anisotropy energy into mechanical
7 tensile stress to the tethered target molecules via two-step processes involving magnetic-to-thermal and
8 thermal-to-mechanical energy transductions. A similar two-step transduction approach using hydrogel
9 optomechanical actuator nanoparticles for controlling mechanoreceptors *in vitro* has been reported previously⁹,
10 but our h-MMA enabled robust deep-tissue stimulation of mechanoreceptors in living organisms using non-
11 invasive and biologically transparent AMF-input. We showed a proof-of-concept study to regulate Notch
12 receptors and downstream synthetic transcription signals, but this generalizable technique can be used to
13 control and understand diverse mechanosensitive receptors in living organisms.

1 ASSOCIATED CONTENT

2 **Supporting Information**

3 Experimental setup for chemical synthesis of hydrogel magnetomechanical actuators (h-MMAs),
4 characterization of h-MMAs, cell line generation and tissue culture, receptor-specific labeling of h-MMAs, *in*
5 *vitro* experiments including h-MMA labeling, AMF stimulation, immunofluorescence staining, and
6 immunoblotting assay, *in vivo* experiment including xenograft generation, *in vivo* h-MMA delivery and AMF
7 stimulation, immunohistochemistry (IHC), and statistical analyses; Figures S1 – S21; Supplementary Note 1
8 for the calculation of IPLP values of h-MMA nanoparticles.

9

10 AUTHOR INFORMATION

11 **Corresponding Author**

12 ***Young-wook Jun**: Department of Otolaryngology, University of California, San Francisco, San Francisco,
13 California 94158, United States; Department of Pharmaceutical Chemistry, University of California, San
14 Francisco, San Francisco, California 94158, United States; Helen Diller Family Cancer Comprehensive Center
15 (HDFCCC), University of California, San Francisco, San Francisco, California 94158, United States; Center
16 for Nanomedicine, Institute for Basic Science (IBS), Seoul 03722, Republic of Korea; Department of Nano
17 Biomedical Engineering (NanoBME), Advanced Science Institute, Yonsei University, Seoul 03722, Republic
18 of Korea; <http://orcid.org/0000-0003-3182-5366>; E-mail: young-wook.jun@ucsf.edu

19 ***Minsuk Kwak**: Center for Nanomedicine, Institute for Basic Science (IBS), Seoul 03722, Republic of
20 Korea; Department of Nano Biomedical Engineering (NanoBME), Advanced Science Institute, Yonsei
21 University, Seoul 03722, Republic of Korea; <http://orcid.org/0000-0002-8095-532X>; E-mail:
22 minsuk.kwak@yonsei.ac.kr

23 ***Jinwoo Cheon**: Center for Nanomedicine, Institute for Basic Science (IBS), Seoul 03722, Republic of
24 Korea; Department of Chemistry, Yonsei University, Seoul 03722, Republic of Korea; Department of Nano
25 Biomedical Engineering (NanoBME), Advanced Science Institute, Yonsei University, Seoul 03722, Republic
26 of Korea; <https://orcid.org/0000-0001-8948-5929>; E-mail: jcheon@yonsei.ac.kr

27

28

1
2
3
4
5
6
7
8
9
10
11
12
13
14
15
16
17
18
19
20
21
22
23
24
25
26
27
28

Authors

Sumin Jeong: Center for Nanomedicine, Institute for Basic Science (IBS), Seoul 03722, Republic of Korea; Department of Chemistry, Yonsei University, Seoul 03722, Republic of Korea; <https://orcid.org/0000-0002-6363-3978>; E-mail: heekyung415@yonsei.ac.kr

Wookjin Shin: Center for Nanomedicine, Institute for Basic Science (IBS), Seoul 03722, Republic of Korea; <https://orcid.org/0000-0002-9135-8643>; E-mail: seramado@yonsei.ac.kr

Mansoo Park: Center for Nanomedicine, Institute for Basic Science (IBS), Seoul 03722, Republic of Korea; Department of Nano Biomedical Engineering (NanoBME), Advanced Science Institute, Yonsei University, Seoul 03722, Republic of Korea; <https://orcid.org/0000-0002-2285-9591>; E-mail: mspark.adm@yonsei.ac.kr

Jung-uk Lee: Center for Nanomedicine, Institute for Basic Science (IBS), Seoul 03722, Republic of Korea; <https://orcid.org/0000-0001-5638-243X>; E-mail: lee7626@yonsei.ac.kr

Yongjun Lim: Center for Nanomedicine, Institute for Basic Science (IBS), Seoul 03722, Republic of Korea; Department of Chemistry, Yonsei University, Seoul 03722, Republic of Korea; <http://orcid.org/0000-0002-7281-7226>; E-mail: yongjun@yonsei.ac.kr

Kunwoo Noh: Center for Nanomedicine, Institute for Basic Science (IBS), Seoul 03722, Republic of Korea; Department of Nano Biomedical Engineering (NanoBME), Advanced Science Institute, Yonsei University, Seoul 03722, Republic of Korea; <https://orcid.org/0009-0006-3138-0861>; E-mail: nkw96@yonsei.ac.kr

Author Contributions

‡S.J. and W.S. contributed equally to this work. Y.J., M.K. and J.C. supervised all aspects of the project. J.H.L., Y.J., and J.C. conceived and designed the project. S.J., J.-u.L., and M.P. designed, synthesized, and characterized nanoparticles. S.J. and W.S. designed and performed the biological experiments and analyzed the data. K.W.N. contributed to the preparation of biological experiments and biomaterials. S.J., Y.J., M.K., and J.C. wrote the manuscript. All authors discussed and commented on the manuscript.

Notes

1 The authors declare no competing financial interests.

2

3 ACKNOWLEDGMENT

4 This work was supported by Institute for Basic Science (IBS-R026-D1) (M.K. and J.C.), by National Research
5 Foundation of Korea (NRF-2021R1F1A1063378) (M.K.), and by the National Institute of Health and the
6 National Institute of General Medical Science (R35GM134948) (Y.J.).

7

8

9 ABBREVIATIONS

10 h-MMA, magnetomechanical actuator; m-Torquer, torque-generating magnetic nanoparticle; MNC, magnetic
11 nanoparticle cluster; pNiPMAM, poly N-isopropylmethacrylamide; VPT, volume-phase-transition; TEM,
12 transmission electron microscope; FCC, face-centered-cubic; AMF, alternating magnetic fields; IPLP,
13 individual particle power loss; DLS, dynamic light scattering; FFT, Fast Fourier Transform; AEM, N-(2-
14 aminoethyl)methacrylate; pAEM, poly-AEM; BG, Benzylguanaine; NICD, Notch intracellular domain; PEG,
15 polyethylene glycol; Dox, doxycycline; IHC, immunohistochemistry; ROI, region of interest.

16

17

1 REFERENCES

- 2 1. Deisseroth, K. Optogenetics. *Nat. Methods* **2011**, *8*, 26.
- 3 2. Toettcher, J. E.; Voigt, C. A.; Weiner, O. D.; Lim, W. A. The Promise of Optogenetics in Cell Biology:
4 Interrogating Molecular Circuits in Space and Time. *Nat. Methods* **2011**, *8*, 35.
- 5 3. Parnas, O.; Jovanovic, M.; Eisenhaure, T. M.; Herbst, R. H.; Dixit, A.; Ye, C. J.; Przybylski, D.; Platt, R.
6 J.; Tirosh, I.; Sanjana, N. E.; Shalem, O.; Satija, R.; Raychowdhury, R.; Mertins, P.; Carr, S. A.; Zhang,
7 F.; Hacohen, N.; Regev, A. A Genome-wide CRISPR Screen in Primary Immune Cells to Dissect
8 Regulatory Networks. *Cell* **2015**, *162* (3), 675.
- 9 4. Gero, M. The Optogenetic Catechism. *Science* **2009**, *326* (5951), 395.
- 10 5. Cogan, S. F. Neural Stimulation and Recording Electrodes. *Annu. Rev. Biomed. Eng.* **2008**, *10*, 275.
- 11 6. Guosong, H.; Lieber, C. M. Novel Electrode Technologies for Neural Recordings. *Nat. Rev. Neurosci.*
12 **2019**, *20* (6), 330.
- 13 7. Sonnen, K. F.; Merten, C. A. Microfluidics as an Emerging Precision Tool in Developmental Biology.
14 *Dev. Cell* **2019**, *48* (3), 293.
- 15 8. Sonnen, K. F.; Lauschke, V. M.; Uraji, J.; Falk, H. J.; Petersen, Y.; Funk, M. C.; Beaupeux, M.; François,
16 P.; Merten, C. A.; Aulehla, A. Modulation of Phase Shift between Wnt and Notch Signaling Oscillations
17 Controls Mesoderm Segmentation. *Cell* **2018**, *172* (5), 1079.
- 18 9. Liu, Z.; Liu, Y.; Chang, Y.; Seyf, H. R.; Henry, A.; Mattheyses, A. L.; Yehl, K.; Zhang, Y.; Huang, Z.;
19 Salaita, K. Nanoscale Optomechanical Actuators for Controlling Mechanotransduction in Living Cells.
20 *Nat. Methods* **2016**, *13* (2), 143.
- 21 10. Tischer, D.; Weiner, O. D. Illuminating Cell Signalling with Optogenetic Tools *Nat. Rev. Mol. Cell Biol.*
22 **2014**, *15* (8), 551.
- 23 11. Zhang, K.; Cui, B. Optogenetic Control of Intracellular Signaling Pathways. *Trends Biotechnol.* **2015**, *33*
24 (2), 92.
- 25 12. All, A. H.; Zeng, X.; Teh, D. B. L.; Yi, Z.; Prasad, A.; Ishizuka, T.; Thakor, N.; Hiromu, Y.; Liu, X.
26 Expanding the Toolbox of Upconversion Nanoparticles for in vivo Optogenetics and Neuromodulation.
27 *Adv. Mater.* **2019**, *31*, 1803474.
- 28 13. Chen, S.; Weitemier, A. Z.; Zeng, X.; He, L.; Wang, X.; Tao, Y.; Huang, A. J. Y.; Hashimoto-dani, Y.;
29 Kano, M.; Iwasaki, H.; Parajuli, L. K.; Okabe, S.; Teh, D. B. L.; All, A. H.; Tsutsui-Kimura, I.; Tanaka,
30 K. F.; Liu, X.; McHugh, T. J. Near-Infrared Deep Brain Stimulation via Upconversion Nanoparticle-
31 Mediated Optogenetics. *Science* **2018**, *359*, 679.
- 32 14. Yi, Z.; All, A. H.; Liu, X. Upconversion Nanoparticle-Mediated Optogenetics. *Adv. Exp. Med. Biol.* **2021**,
33 *1293*, 641.

- 1 15. Ao, Y.; Zeng, K.; Yu, B.; Miao, Y.; Hung, W.; Yu, Z.; Xue, Y.; Tan, T. T. Y.; Xu, T.; Zhen, M.; Yang,
2 X.; Zhang, Y.; Gao, S. An Upconversion Nanoparticle Enables Near Infrared-Optogenetic Manipulation
3 of the *Caenorhabditis Elegans* Motor Circuit. *ACS Nano* **2019**, *13* (3), 3373.
- 4 16. Chen, R.; Romero, G.; Christiansen, M. G.; Mohr, A.; Anikeeva, P. Wireless Magnetothermal Deep Brain
5 Stimulation. *Science* **2015**, *347* (6229), 1477.
- 6 17. Su, H.; Brockman, J. M.; Duan, Y.; Sen, N.; Chhabra, H.; Bazrafshan, A.; Blanchard, A. T.; Meyer, T.;
7 Andrews, B.; Doye, J. P. K.; Ke, Y.; Dyer, R. B.; Salaita, K. Massively Parallelized Molecular Force
8 Manipulation with On-Demand Thermal and Optical Control. *J. Am. Chem. Soc.* **2021**, *143* (46), 19466.
- 9 18. Kwizera, E. A.; Stewart, S.; Mahmud, M. M.; He, X. Magnetic Nanoparticle-Mediated Heating for
10 Biomedical Applications. *J. Heat Transfer* **2022**, *144* (3), 030801.
- 11 19. Romero, G.; Christiansen, M. G.; Barbosa, L. S.; Garcia, F.; Anikeeva, P. Localized Excitation of Neural
12 Activity via Rapid Magnetothermal Drug Release. *Adv. Funct. Mater.* **2016**, *26*, 6471.
- 13 20. Rosenfeld, D.; Senko, A. W.; Moon, J.; Yick, I.; Varnavides, G.; Gregurec, D.; Koehler, F.; Chiang, P. H.;
14 Christiansen, M. G.; Maeng, L. Y.; Widge, A. S.; Anikeeva, P. Transgene-Free Remote Magnetothermal
15 Regulation of Adrenal Hormones. *Sci. Adv.* **2020**, *6*, eaaz3734.
- 16 21. Maresca, D.; Lakshmanan, A.; Abedi, M.; Bar-Zion, A.; Farhadi, A.; Lu, G. J.; Szablowski, J. O.; Wu, D.;
17 Yoo, S.; Shapiro, M. G. Biomolecular Ultrasound and Sonogenetics. *Annu. Rev. Chem. Biomol. Eng.*
18 **2018**, *9*, 229.
- 19 22. Fan, C. H.; Wei, K. C.; Chiu, N. H.; Liao, E. C.; Wang, H. C.; Wu, R. Y.; Ho, Y. J.; Chan, H. L.; Wang,
20 T. S. A.; Huang, Y. Z.; Hsieh, T. H.; Lin, C. H.; Lin, Y. C.; Yeh, C. K. Sonogenetic-Based
21 Neuromodulation for the Amelioration of Parkinson's Disease. *Nano Lett.* **2021**, *21* (14), 5967.
- 22 23. Zhu, L.; Wu, Y.; Yoon, C. W.; Wang, Y. Mechanogenetics for Cellular Engineering and Cancer
23 Immunotherapy. *Curr. Opin. Biotechnol.* **2020**, *66*, 88.
- 24 24. Seo, D.; Southard, K. M.; Kim, J. W.; Lee, H. J.; Farlow, J.; Lee, J. U.; Litt, D. B.; Haas, T.; Alivisatos, A.
25 P.; Cheon, J.; Gartner, Z. J.; Jun, Y. W. A Mechanogenetic Toolkit for Interrogating Cell Signaling in
26 Space and Time. *Cell* **2016**, *165*, 1507.
- 27 25. Perlmutter, J. S.; Mink, J. W. Deep Brain Stimulation. *Annu. Rev. Neurosci.* **2006**, *29*, 229.
- 28 26. Montgomery, K. L. Yeh, A. J.; Ho, J. S.; Tsao, V.; Iyer, S. M.; Grosenick, L.; Ferenczi, E. A.; Tanabe, Y.;
29 Deisseroth, K.; Delp, S. L.; Poon, A. S. Y. Wirelessly Powered, Fully Internal Optogenetics for Brain,
30 Spinal and Peripheral Circuits in Mice. *Nat. Methods* **2015**, *12* (10), 969.
- 31 27. Kim, J. W.; Seo, D.; Lee, J. U.; Southard, K. M.; Lim, Y.; Kim, D.; Gartner, Z. J.; Jun, Y. W.; Cheon, J.
32 Single-Cell Mechanogenetics Using Monovalent Magnetoplasmonic Nanoparticles. *Nat. Protoc.* **2017**, *12*,
33 1871.

- 1 28. Kwak, M.; Gu, W.; Jeong, H.; Lee, H.; Lee, J. U.; An, M.; Kim, Y. H.; Lee, J. H.; Cheon, J.; Jun, Y. W.
2 Small, Clickable, and Monovalent Magnetofluorescent Nanoparticles (MFNs) Enable Mechanogenetic
3 Regulation of Receptors in a Crowded Live Cell Microenvironment. *Nano Lett.* **2019**, *19*, 3761.
- 4 29. Stanley, S. A.; Kelly, L.; Latcha, K. N.; Schmidt, S. F.; Yu, X.; Nectow, A. R.; Sauer, J.; Dyke, J. P.;
5 Dordick, J. S.; Friedman, J. M. Bidirectional Electromagnetic Control of the Hypothalamus Regulates
6 Feeding and Metabolism. *Nature* **2016**, *531* (7596), 647.
- 7 30. Munshi, R.; Qadri, S. M.; Zhang, Q.; Rubio, I. C.; Pino, P.; Pralle, A. Magnetothermal Genetic Deep
8 Brain Stimulation of Motor Behaviors in Awake, Freely Moving Mice. *Elife* **2017**, *6*, e27069.
- 9 31. Lee, J. U.; Shin, W.; Lim, Y.; Kim, J.; Kim, W. R.; Kim, H.; Lee, J. H.; Cheon, J. Non-Contact Long-
10 Range Magnetic Stimulation of Mechanosensitive Ion Channels in Freely Moving Animals. *Nat. Mater.*
11 **2021**, *20*, 1029.
- 12 32. Shin, W.; Jeong, S.; Lee, J. U.; Jeong, S. Y.; Shin, J.; Kim, H. H.; Cheon, J.; Lee, J. H. Magnetogenetics
13 with Piezo1 Mechanosensitive Ion Channel for CRISPR Gene Editing. *Nano Lett.* **2022**, *22* (18), 7415.
- 14 33. Wang, X.; Ha, T. J. Defining Single Molecular Forces Required to Activate Integrin and Notch Signaling.
15 *Science* **2013**, *340* (6135), 991.
- 16 34. Jo, M. H.; Li, J.; Jaumouillé, V.; Hao, Y.; Coppola, J.; Yan, J.; Waterman, C. M.; Springer, T. A.; Ha, T.
17 J. Single-Molecule Characterization of Subtype-Specific β 1 Integrin Mechanics. *Nat. Commun.* **2022**, *13*
18 (1), 7471.
- 19 35. Dutta, P. K.; Zhang, Y.; Blanchard, A. T.; Ge, C.; Rushdi, M.; Weiss, K.; Zhu, C.; Ke, Y.; Salaita, K.
20 Programmable Multivalent DNA-Origami Tension Probes for Reporting Cellular Traction Forces. *Nano*
21 *Lett.* **2018**, *18*, 4803.
- 22 36. Ramey-Ward, A. N.; Su, H.; Salaita, K. Mechanical Stimulation of Adhesion Receptors Using Light-
23 Responsive Nanoparticle Actuators Enhances Myogenesis. *ACS Appl. Mater. Interfaces* **2020**, *12* (32),
24 35903.
- 25 37. Hong, J.; Ge, C.; Jothikumar, P.; Yuan, Z.; Liu, B.; Bai, K.; Li, K.; Rittase, W.; Shinzawa, M.; Zhang, Y.;
26 Palin, A.; Love, P.; Yu, X.; Salaita, K.; Evavold, B. D.; Singer, A.; Zhu, C. A TCR Mechanotransduction
27 Signaling Loop Induces Negative Selection in the Thymus. *Nat. Immunol.* **2018**, *19*, 1379.
- 28 38. Chen, Y.; Li, Z.; Ju, L. A. Tensile and Compressive Force Regulation on Cell Mechanosensing. *Biophys.*
29 *Rev.* **2019**, *11*, 311.
- 30 39. Périgo, E. A.; Hemery, G.; Sandre, O.; Ortega, D.; Garaio, E.; Plazaola, F.; Teran, F. J. Fundamentals and
31 Advances in Magnetic Hyperthermia. *Appl. Phys. Rev.* **2015**, *2*, 041302.
- 32 40. Sebesta, C.; Hinojosa, D. T.; Wang, B.; Asfour, J.; Li, Z.; Duret, G.; Jiang, K.; Xiao, Z.; Zhang, L.;
33 Zhang, Q.; Colvin, V. L.; Goetz, S. M.; Peterchev, A. V.; Dierick, H. A.; Bao, G.; Robinson, J. T.

- 1 Subsecond Multichannel Magnetic Control of Select Neural Circuits in Freely Moving Flies. *Nat. Mater.*
2 **2022**, *21*, 951.
- 3 41. Rosensweig, R. E. Heating Magnetic Fluid with Alternating Magnetic Field. *J. Magn. Magn. Mater.* **2002**,
4 *252*, 370.
- 5 42. Lee, J. H.; Jang, J. T.; Choi, J. S.; Moon, S. H.; Noh, S. H.; Kim, J. W.; Kim, J. G.; Kim, I. S.; Park, K. I.;
6 Cheon, J. Exchange-Coupled Magnetic Nanoparticles for Efficient Heat Induction. *Nat. Nanotechnol.*
7 **2011**, *6*, 418.
- 8 43. Jang, J. T.; Nah, H.; Lee, J. H.; Moon, S. H.; Kim, M. G.; Cheon, J. Critical Enhancements of MRI
9 Contrast and Hyperthermic Effects by Dopant-Controlled Magnetic Nanoparticles. *Angew. Chem. Int. Ed.*
10 *Engl.* **2009**, *48*, 1234.
- 11 44. Cardellini, A.; Fasano, M.; Bigdeli, M. B.; Chiavazzo, E.; Asinari, P. Thermal Transport Phenomena in
12 Nanoparticle Suspensions. *J. Phys. Condens. Matter* **2016**, *28*, 483003.
- 13 45. Obaidat, I. M.; Issa, B.; Haik, Y. Magnetic Properties of Magnetic Nanoparticles for Efficient
14 Hyperthermia. *Nanomaterials* **2015**, *5* (1), 63.
- 15 46. Shubitidze, F.; Kekalo, K.; Stigliano, R.; Baker, I. Magnetic Nanoparticles with High Specific Absorption
16 Rate of Electromagnetic Energy at Low Field Strength for Hyperthermia Therapy. *J. Appl. Phys.* **2015**,
17 *117*, 094302.
- 18 47. Cobianchi, M.; Guerrini, A.; Avolio, M.; Innocenti, C.; Corti, M.; Arosio, P.; Orsini, F.; Sangregorio, C.;
19 Lascialfari, A. Experimental Determination of the Frequency and Field Dependence of Specific Loss
20 Power in Magnetic Fluid Hyperthermia. *J. Magn. Magn. Mater.* **2017**, *444*, 154.
- 21 48. Mohapatra, J.; Xing, M.; Liu, J. P. Inductive Thermal Effect of Ferrite Magnetic Nanoparticles. *Materials*
22 **2019**, *12* (19), 3208.
- 23 49. Rytov, R. A.; Bautin, V. A.; Usov, N. A. Towards Optimal Thermal Distribution in Magnetic
24 Hyperthermia. *Sci. Rep.* **2022**, *12*, 3023.
- 25 50. Christiansen, M. G.; Senko, A. W.; Chen, R.; Romero, G.; Anikeeva, P. Magnetically Multiplexed
26 Heating of Single Domain Nanoparticles. *Appl. Phys. Lett.* **2014**, *104*, 213103.
- 27 51. Ovejero, J. G.; Armenia, I.; Serantes, D.; Veintemillas-Verdaguer, S.; Zeballos, N.; López-Gallego, F.;
28 Grüttner, C.; Fuente, J. M.; Morales, M. P.; Grazu, V. Selective Magnetic Nanoheating: Combining Iron
29 Oxide Nanoparticles for Multi-Hot-Spot Induction and Sequential Regulation. *Nano Lett.* **2021**, *21*, 7213.
- 30 52. Stolarczyk, J. K.; Deak, A.; Brougham, D. F. Nanoparticle Clusters: Assembly and Control Over Internal
31 Order, Current Capabilities, and Future Potential. *Adv. Mater.* **2016**, *28*, 5400.
- 32 53. Singamaneni, S.; Bliznyuk, V. N.; Binek, C.; Tsymbal, E. Y. Magnetic Nanoparticles: Recent Advances
33 in Synthesis, Self-Assembly and Applications. *J. Mater. Chem.* **2011**, *21*, 16819.

- 1 54. Polo-Corrales, L.; Rinaldia, C. Monitoring Iron Oxide Nanoparticle Surface Temperature in an
2 Alternating Magnetic Field Using Thermoresponsive Fluorescent Polymers. *J. Appl. Phys.* **2012**, *111*,
3 07B334.
- 4 55. Guibert, C.; Dupuis, V.; Peyre, V.; Fresnais, J. Hyperthermia of Magnetic Nanoparticles: Experimental
5 Study of the Role of Aggregation. *J. Phys. Chem. C. Nanomater. Interfaces* **2015**, *119* (50), 28148.
- 6 56. Serantes, D.; Simeonidis, K.; Angelakeris, M.; Chubykalo-Fesenko, O.; Marciello, M.; Morales, M. D. P.;
7 Baldomir, D.; Martinez-Boubeta, C. Multiplying Magnetic Hyperthermia Response by Nanoparticle
8 Assembling. *J. Phys. Chem. C Nanomater. Interfaces* **2014**, *118* (11), 5927.
- 9 57. Sakellari, D.; Brintakis, K.; Kostopoulou, A.; Myrovali, E.; Simeonidis, K.; Lappas, A.; Angelakeris, M.
10 Ferrimagnetic Nanocrystal Assemblies as Versatile Magnetic Particle Hyperthermia Mediators. *Mater.*
11 *Sci. Eng. C* **2016**, *58*, 187.
- 12 58. Zhao, J.; Su, H.; Vansuch, G. E.; Liu, Z.; Salaita, K.; Dyer, R. B. Localized Nanoscale Heating Leads to
13 Ultrafast Hydrogel Volume-Phase Transition. *ACS Nano* **2019**, *13* (1), 515.
- 14 59. Dong, Y.; Bazrafshan, A.; Pokutta, A.; Sulejmani, F.; Sun, W.; Combs, J. D.; Clarke, K. C.; Salaita, K.
15 Chameleon-Inspired Strain-Accommodating Smart Skin. *ACS Nano* **2019**, *13*, 9918.
- 16 60. Su, H.; Liu, Z.; Liu, Y.; Ma, V. P.; Blanchard, A.; Zhao, J.; Galior, K.; Dyer, R. B.; and Salaita, K. Light-
17 Responsive Polymer Particles as Force Clamps for the Mechanical Unfolding of Target Molecules. *Nano*
18 *Lett.* **2018**, *18*, 2630.
- 19 61. Huang, H.; Delikanli, S.; Zeng, H.; Ferkey, D. M.; Pralle, A. Remote Control of Ion Channels and
20 Neurons through Magnetic-Field Heating of Nanoparticles. *Nat. Nanotechnol.* **2010**, *5*, 602.
- 21 62. Nai, J.; Wang, S.; Lou, X. W. D. Ordered Colloidal Clusters Constructed by Nanocrystals with Valence
22 for Efficient CO₂ Photoreduction. *Sci. Adv.* **2019**, *5*, eaax5095.
- 23 63. Teich, E. G.; Anders, G. V.; Klotsa, D.; Dshemuchadse, J.; Glotzer, S. C. Clusters of Polyhedra in
24 Spherical Confinement. *Proc. Natl. Acad. Sci. U. S. A.* **2016**, *113* (6), E669.
- 25 64. Ganesan, V.; Lahiri, B. B.; Louis, C.; Philip, J.; Damodaran, S. P. Size-Controlled Synthesis of
26 Superparamagnetic Magnetite Nanoclusters for Heat Generation in an Alternating Magnetic Field. *J. Mol.*
27 *Liq.* **2019**, *281*, 315.
- 28 65. Wang, Y.; Xu, F.; Zhang, C.; Lei, D.; Tang, Y.; Xu, H.; Zhang, Z.; Lu, H.; Du, X.; Yang, G. Y. High MR
29 Sensitive Fluorescent Magnetite Nanocluster for Stem Cell Tracking in Ischemic Mouse Brain.
30 *Nanomedicine.* **2011**, *7*, 1009.
- 31 66. Isojima, T.; Suh, S. K.; Vander Sande, J. B.; Hatton, T. A. Controlled Assembly of Nanoparticle
32 Structures: Spherical and Toroidal Superlattices and Nanoparticle-Coated Polymeric Beads. *Langmuir*
33 **2009**, *25* (14), 8292.

- 1 67. Fu, R.; Jin, X.; Liang, J.; Zheng, W.; Zhuang, J.; Yang, W. Preparation of Nearly Monodispersed
2 Fe₃O₄/SiO₂ Composite Particles from Aggregates of Fe₃O₄ Nanoparticles. *J. Mater. Chem.* **2011**, *21*,
3 15352.
- 4 68. Ramey-Ward, A. N.; Su, H.; Salaita, K. Mechanical Stimulation of Adhesion Receptors Using Light-
5 Responsive Nanoparticle Actuators Enhances Myogenesis. *ACS Appl. Mater. Interfaces* **2020**, *12* (32),
6 35903.
- 7 69. Lim, Y.; Noh, S. H.; Shin, T. H.; Lee, J. U.; Lungerich, D.; Lee, J. H.; Cheon, J. Magnetothermally
8 Activated Nanometer-level Modular Functional Group Grafting of Nanoparticles. *Nano Lett.* **2021**, *21*,
9 3649.
- 10 70. Azo Polymerization Initiators Comprehensive Catalog. FUJIFILM Wako Pure Chemical Corporation.
- 11 71. Riedinger, A.; Guardia, P.; Curcio, A.; Garcia, M. A.; Cingolani, R.; Manna, L.; Pellegrino, T.
12 Subnanometer Local Temperature Probing and Remotely Controlled Drug Release Based on Azo-
13 Functionalized Iron Oxide Nanoparticles. *Nano Lett.* **2013**, *13*, 2399.
- 14 72. Kopan, R.; Ilagan, X. G. The Canonical Notch Signaling Pathway: Unfolding the Activation Mechanism.
15 *Cell* **2009**, *137* (2) 216.
- 16 73. Gordon, W. R.; Zimmerman, B.; He, L.; Miles, L. J.; Huang, J.; Tiyanont, K.; McArthur, D. G.; Aster, J.
17 C.; Perrimon, N.; Loparo, J. J.; Blacklow, S. C. Mechanical Allostery: Evidence for a Force Requirement
18 in the Proteolytic Activation of Notch. *Dev. Cell* **2015**, *33* (6), 729.
- 19 74. Tagami, S.; Okochi, M.; Yanagida, K.; Ikuta, A.; Fukumori, A.; Matsumoto, N.; Ishizuka-Katsura, Y.;
20 Nakayama, T.; Itoh, N.; Jiang, J.; Nishitomi, K.; Kamino, K.; Morihara, T.; Hashimoto, R.; Tanaka, T.;
21 Kudo, T.; Chiba, S.; Takeda, M. Regulation of Notch Signaling by Dynamic Changes in the Precision of
22 S3 Cleavage of Notch-1. *Mol. Cell Biol.* **2008**, *28*, 165.
- 23

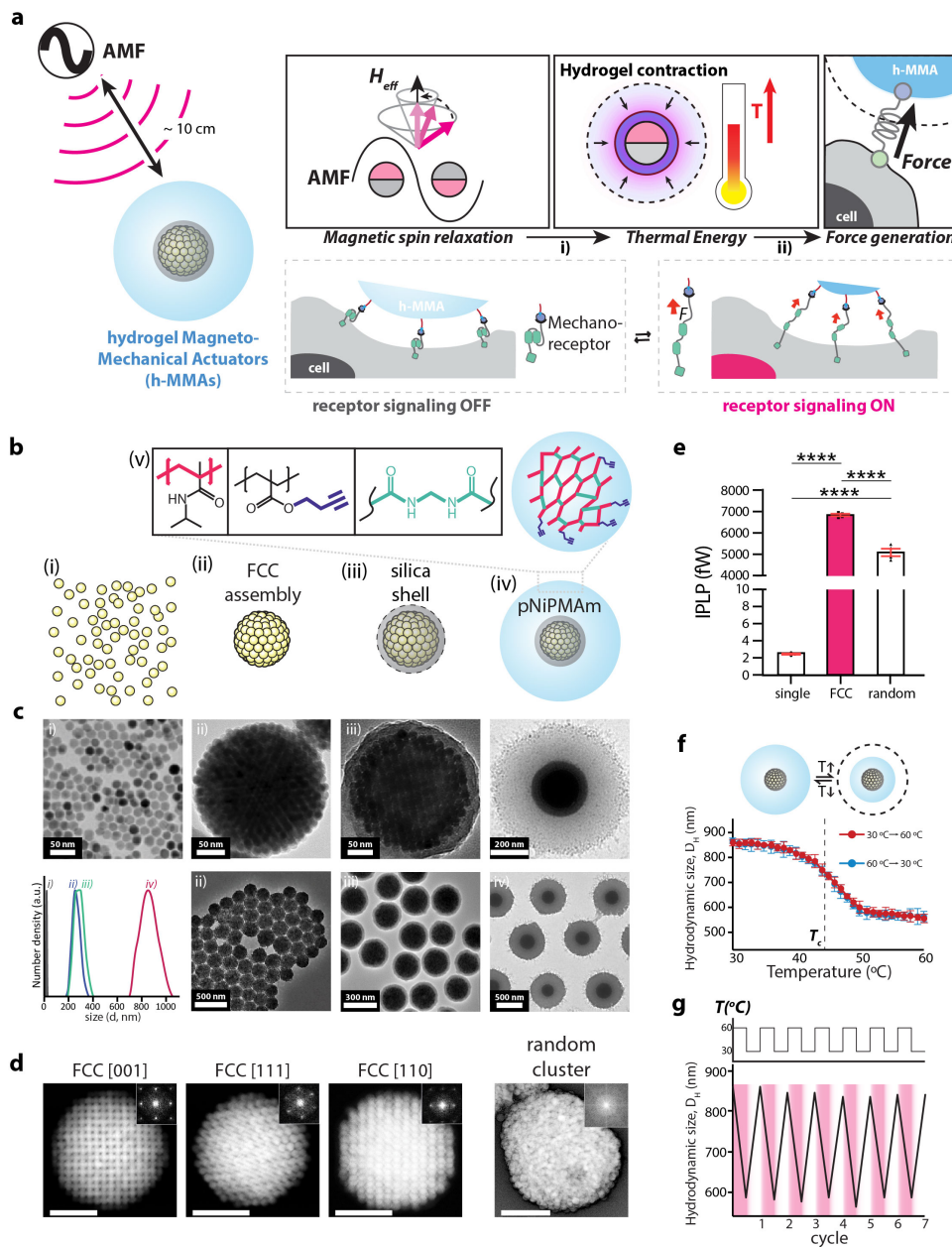


Figure 1. Design, synthesis, and characterization of hydrogel magnetomechanical actuator (h-MMA) nanoparticles. (a) Schematic illustration showing wireless control of targeted mechanoreceptors using h-MMAs. h-MMAs exert mechanical tensile stress to target proteins in response to alternating magnetic fields via a 2-step mechanism including i) magnetic-to-thermal and ii) thermal-to-mechanical transductions. (b, c) Schematics and TEM images of i) 13 nm Zn-doped iron oxide ($Zn_{0.4}Fe_{2.6}O_4$) nanoparticles, ii) magnetic nanoparticle clusters (MNCs) in a face-centered cubic (FCC) superlattice structure, iii) MNC@SiO₂, and iv) MNC@SiO₂@pNiPMAm. v) Surface functionalization of h-MMAs with pNiPMAm polymer and alkyne functional group cross-linked by N, N'-methylenebisacrylamide. DLS spectra at each stage of h-MMA synthesis is also shown in the inset. (d) Scanning TEM images and reduced FFT images (insets) of an FCC cluster at different crystalline faces and of a random cluster. Scale bars = 100 nm. (e) Individual particle loss power (IPLP) values of single MNPs, FCC-structured MNCs, and random aggregates. Data are mean \pm s.e.m. from $n = 4$ independent trials (**** $p < 0.0001$; one-way ANOVA followed by Tukey's). (f) Temperature-dependent VPT of h-MMAs. The critical temperature (T_c) is marked with a black dotted line (43 ± 0.5 °C, $n = 3$). (g) Measurement of the hydrodynamic size of h-MMAs through temperature-controlled DLS measurement during 7 cycles of repeated heating and cooling.

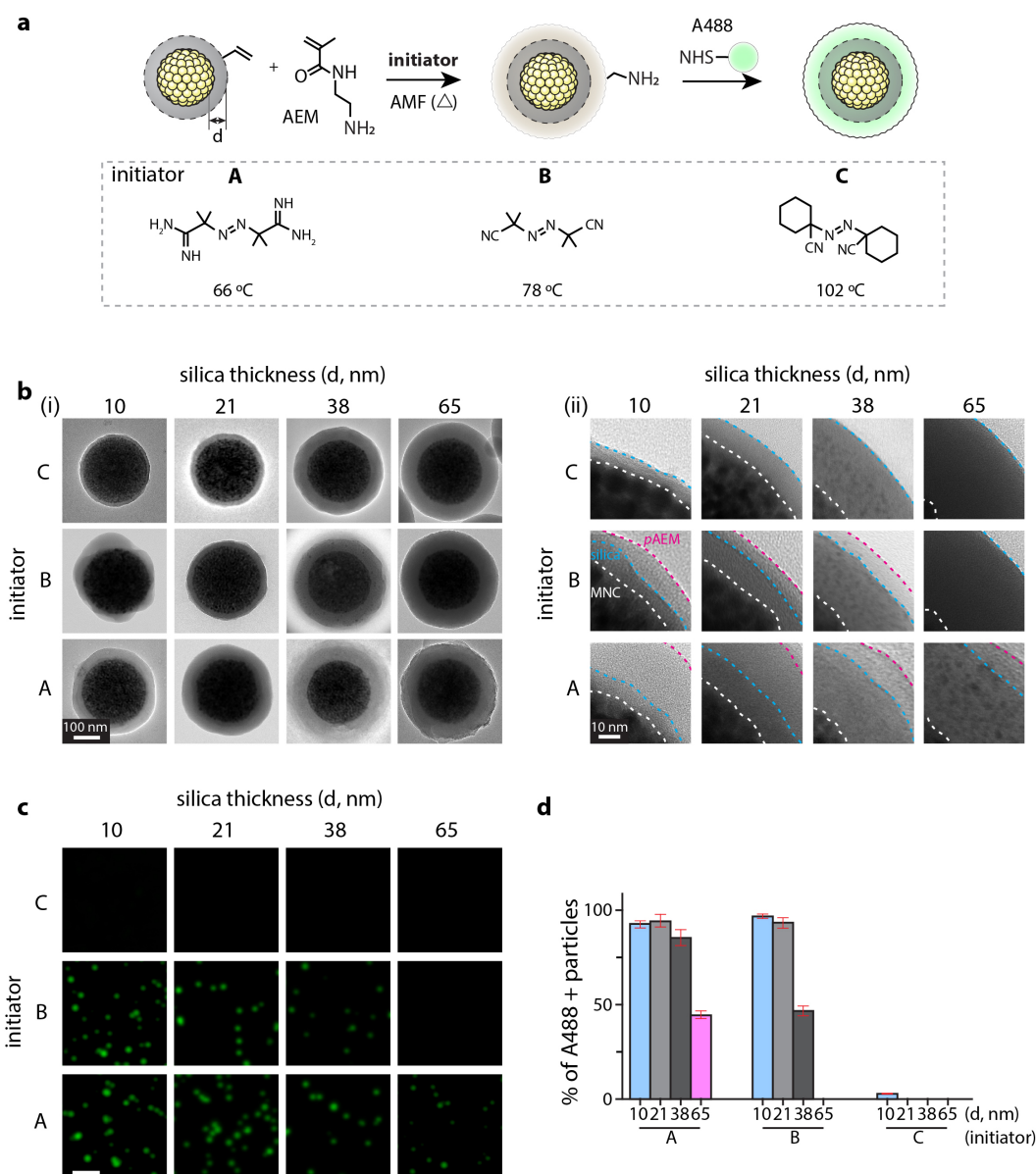


Figure 2. Thermal polymerization of N-(2-aminoethyl)methacrylate (AEM) on MNC@SiO₂ to investigate AMF-induced local heating effects by MNCs. (a) (top) Schematic illustrations of radical polymerization of AEM and subsequent conjugation of amine-reactive fluorescence dyes within it. We varied the SiO₂ layer thickness ($d = 10, 21, 38, 65$ nm) to investigate distance-dependent thermal decay from MNC surface. (bottom) Three thermo-labile azo-molecule initiators with varied decomposition temperatures for AEM polymerization: A, 2,2'-azobis(2-methylpropionamide) dihydrochloride; B, 2,2'-azobis(2-methylpropionitrile); C, 1,1'-azobis(cyclohexanecarbonitrile). (b) Representative TEM images (Left: entire particle view, Right: zoom-in view) after AMF-stimulation in presence of respective MNC@SiO₂ particles and initiators. Scale bar = 100 nm. Interface of MNC/SiO₂, SiO₂/pAEM, and AEM/vacuum (white dotted line) are marked by white, blue, magenta dotted lines, respectively. Scale bar = 10 nm. (c) Fluorescence signals of the Alexa488-positive particles prepared with radical polymerization conditions shown in Figure 2b and subsequent conjugation of A488-NHS. The images were acquired with a 488-nm laser and FITC emission filter. Scale bar = 2 μ m. (d) Fraction analysis of A488-positive particles. Fluorescence-positive particles were identified by using a threshold calculated as mean \pm 3 \times SD of basal signal intensity. Data are mean \pm SD from $n = 3$ independent experiments.

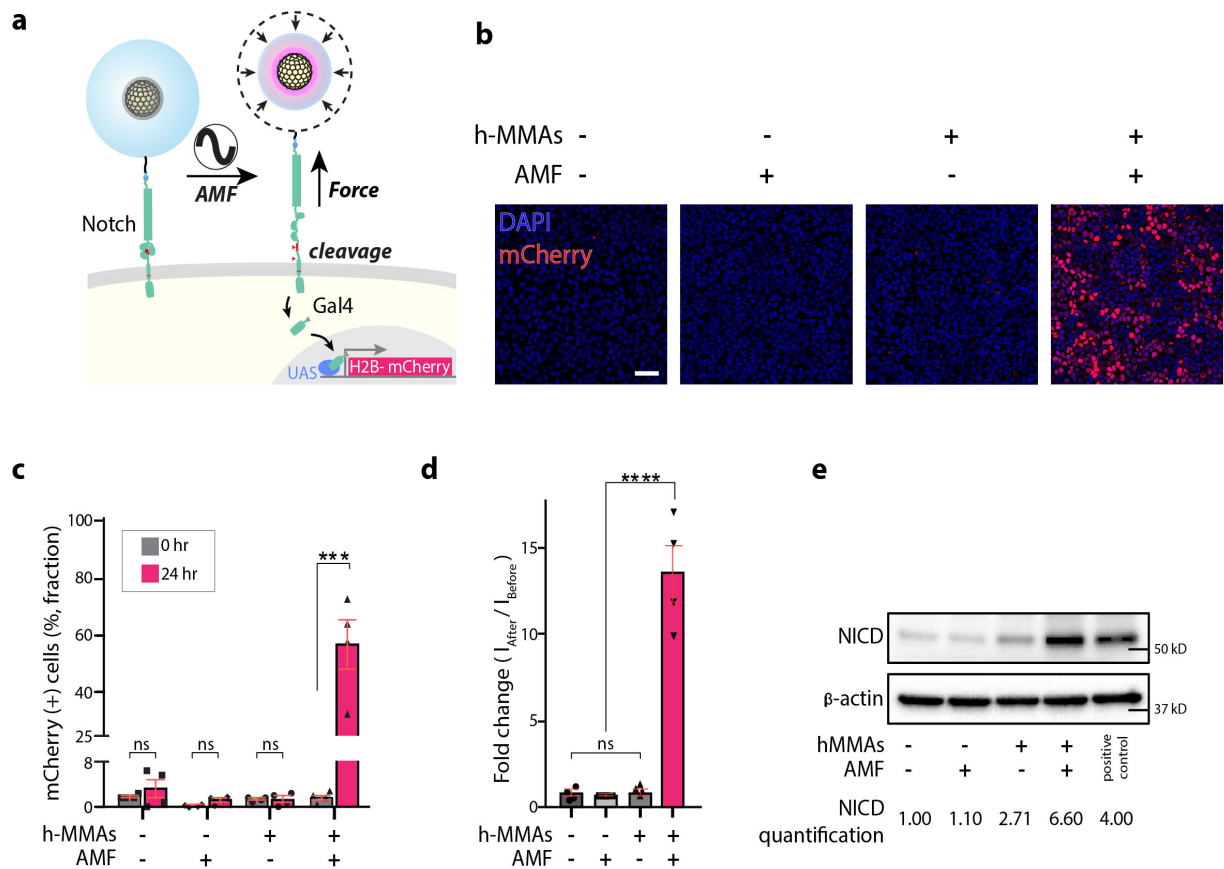


Figure 3. AMF-induced activation of Notch signaling in a cell line model using h-MMA nanoparticles. (a) A schematic illustration of h-MMAs induced activation of U2OS reporter cells expressing SNAP-Notch1-Gal4 and H2B-mCherry. h-MMAs specifically label Notch1 receptors via SNAP-benzylguanine (BG) chemistry. AMF stimulation (50 kHz at 500 Oe, 30 s ON / 2 min OFF cycle for 15 times) induced VPT and exerted mechanical force to Notch1. Mechanical stimulation of Notch1 triggers enzymatic cleavages of Notch1 and downstream transcription of H2B-mCherry. (b) Representative confocal fluorescence images of the reporter cells treated with h-MMA nanoparticles and AMF. Cells treated with no h-MMA or AMF were used as controls. Scale bar = 100 μ m. (c) Percentage of the mCherry-positive cells with or without AMF stimulation or h-MMA treatment. Fluorescence-positive fractions were measured at (0 hr) and 24-hr post stimulation. Data are mean \pm SD from n = 4 biological replicates (ns, non-significant; ***p < 0.001; two-tailed Student's t-test). (d) Normalized fold-change in mCherry fluorescence signal observed at 24-hr post-AMF stimulation as compared to the baseline level for respective experimental conditions. Data are mean \pm SD from n = 4 biological replicates (ns, non-significant; ****p < 0.0001; two-tailed Student's t-test). (e) Immunoblot analysis of cleaved Notch intracellular domain (NICD). β -actin levels represent the loading control. The number below the gel images indicates the relative NICD band intensity. The intensity of each NICD band relative to the respective β -actin band was quantified and normalized to that of the control groups treated with no h-MMAs or AMF.

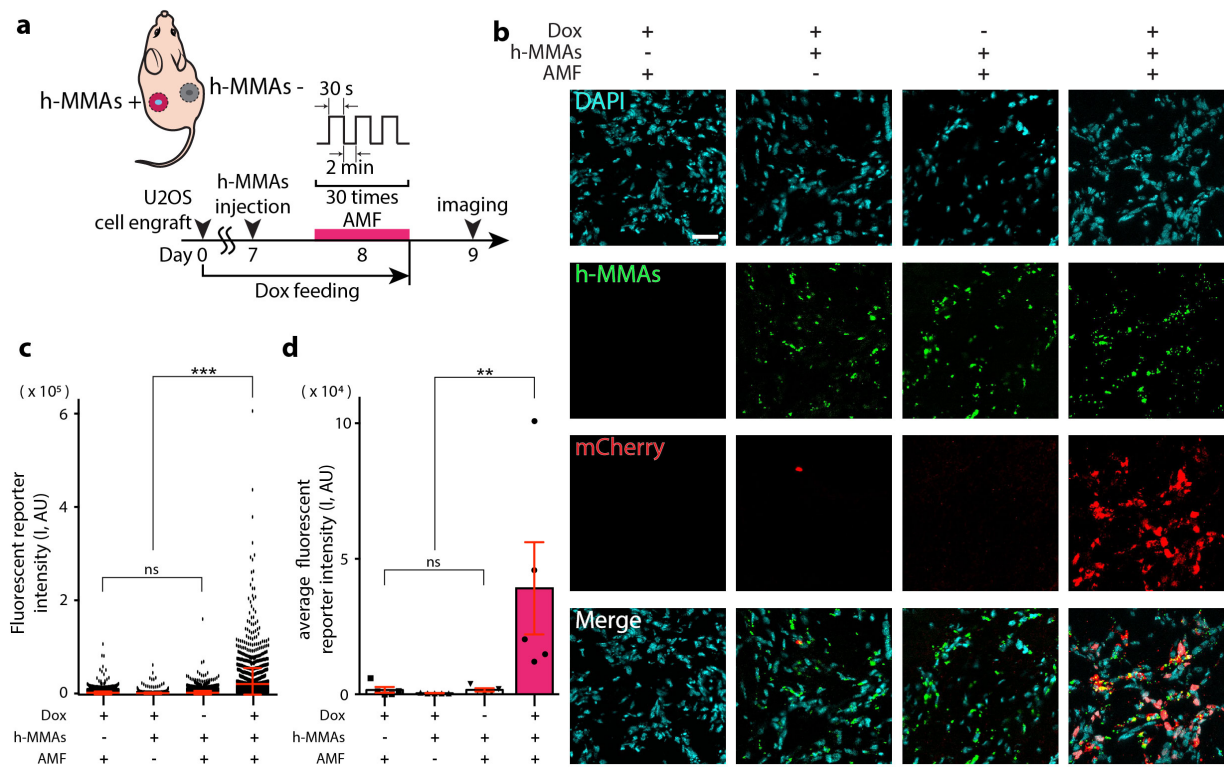


Figure 4. Minimally invasive remote control of cells expressing Notch receptors using h-MMA nanoparticles.

(a) A schematic illustration of AMF-induced h-MMA stimulation using a xenograft mouse model. Fluorescent reporter Notch1-U2OS cells were implanted on both sides of the mice on day 0. Mice were provided with a doxycycline (Dox, 2 mg/ml) diet for Notch receptor expression. One week later, h-MMAs were directly injected into the center of the xenograft, and AMF was applied to the xenograft position. On Day 9, mice were sacrificed and cryosectioned tissues were prepared for immunohistochemical analyses. (b) Representative confocal fluorescence images of tumor sections with AMF and h-MMA treatment. Substantial mCherry (red) expression was observed only in the presence of h-MMAs (green), Dox treatment, and AMF. DAPI (blue), Scale bar = 40 μ m. Tumors with no AMF or h-MMA treatments were used as negative controls. (c) Quantification of nuclear mCherry signal per single cell in the representative slices where h-MMAs were localized. Data are mean \pm s.e.m. from $n = 2,300$ cells from 5 animals (ns, non-significant; *** $p < 0.005$; one-way ANOVA followed by Tukey's). (d) Quantification of average nuclear mCherry fluorescence intensity. Data are mean \pm SD from $n = 5$ animals (ns, non-significant; ** $p < 0.005$; one-way ANOVA followed by Tukey's).

1

2

TOC Graphic

